MoS2 Defect Healing for High-Performance Chemical Sensing of Polycyclic Aromatic Hydrocarbons

Fernando Jimenez Urbanos, Sara Gullace, Paolo Samorì

▶ **To cite this version:**

Fernando Jimenez Urbanos, Sara Gullace, Paolo Samorì. MoS2 Defect Healing for High-Performance Chemical Sensing of Polycyclic Aromatic Hydrocarbons. ACS Nano, 2022, 16 (7), pp.11234-11243. 10.1021/acsnano.2c04503 . hal-03752542

HAL Id: hal-03752542
https://hal.science/hal-03752542v1

Submitted on 16 Aug 2022

HAL is a multi-disciplinary open access archive for the deposit and dissemination of scientific research documents, whether they are published or not. The documents may come from teaching and research institutions in France or abroad, or from public or private research centers.

L'archive ouverte pluridisciplinaire **HAL**, est destinée au dépôt et à la diffusion de documents scientifiques de niveau recherche, publiés ou non, émanant des établissements d'enseignement et de recherche français ou étrangers, des laboratoires publics ou privés.

MoS_2 Defect Healing for High-Performance Chemical Sensing of Polycyclic Aromatic Hydrocarbons

Fernando J. Urbanos‡, Sara Gullace‡, and Paolo Samorì*

University of Strasbourg CNRS, ISIS UMR 7006, 8 Allée Gaspard Monge, Strasbourg, F-67000, France

ABSTRACT: The increasing population and industrial development are responsible for the environmental pollution. Among toxic chemicals, polycyclic aromatic hydrocarbons (PAHs) are highly carcinogenic contaminants resulting from the incomplete combustion of organic materials. Two-dimensional materials, such as transition metal dichalcogenides (TMDCs), are ideal sensory scaffolds, combining high surface-to-volume ratio with physical and chemical properties that are strongly susceptible to environmental changes. TMDCs can be integrated in field-effect transistors (FETs), which can operate as high-performance chemical detectors of (non-)covalent interaction with small molecules. Here, we have developed MoS_2-based FETs as platforms for PAHs sensing, relying on the affinity of the planar polyaromatic molecules for the basal plane of MoS_2 and the structural defects in its lattice. X-ray photoelectron spectroscopy analysis, photoluminescence measurements and transfer characteristics showed a notable reduction in the defectiveness of MoS_2 and a p-type doping upon exposure to PAHs solutions, with a magnitude determined by the correlation between the ionization energies (E_I) of the PAH and that of MoS_2. Naphthalene, endowed with the higher E_I among the studied PAHs, exhibited the highest output. We observed a log-log correlation between MoS_2 doping and naphthalene concentration in water in a wide range (10^{-9}-10^{-6} M), as well as a reversible response to the analyte. Naphthalene concentrations as low as 0.128 ppb were detected, being below the limits imposed by health regulations for drinking water. Furthermore, our MoS_2 devices can reversibly detect vapors of naphthalene both with an electrical and optical readout, confirming that our architecture could operate as a dual sensing platform.

KEYWORDS: transition metal dichalcogenides, MoS_2, polycyclic aromatic hydrocarbons, field-effect transistors, defect healing, doping, sensing.

The contamination of soil, water sources and air, resulting from the rapid industrial development and the growing world population, has become a major worldwide concern.[1-4] Fast and precise sensors for air and water quality monitoring are required for tracking the activity of power plants, oil and gas industries, with a specific focus on their impact on nature. This monitoring can take place *via* the identification and quantification of trace concentrations of toxic heavy elements and molecular contaminants.[5] Among all the possible pollutants, polycyclic aromatic hydrocarbons (PAHs) have been identified by the United States Environmental Protection Agency (EPA) as a potential cause of serious health problems, such as red blood cell damage leading to anemia, suppressed immune system, developmental and reproductive effects, and cancer.[6-8] Because of this reason, their maximum concentration in drinking water has been set to 0.2 ppb. Similarly, the European Parliament and Council included PAHs, and especially naphthalene, in the list of the priority substances that pose a significant risk to or *via* the aquatic and air environments. Since PAHs usually originate from emissions from coal-, oil-, and wood-burning stoves, furnaces in incinerators and asphalt processing, their permissible air exposure level in the workplace has been limited to 0.2 mg/m^3 by the Occupational Safety and Health Administration (OSHA). Hitherto, the most common techniques for the detection of PAHs are based on expensive and non-selective methods, such as the Chelsea UviLux fluorometers employed to monitor the presence of fluorescent contaminants in natural waters with high sensitivity but no selectivity. Considerable research effort has been devoted to the development of new sensing protocols, most of them being time-consuming, requiring expensive techniques[9,10] and prior cumbersome functionalization of the sensing device as a route to attain selectivity *via* the supramolecular recognition of the analyte.[11,12] Stanley *et al.* proposed the detection of PAHs using a quartz microbalance functionalized with aminethiols monolayers carrying an anthracene group in order to achieve a preferential detection of anthracene, with a sensitivity of 2 ppb.[13] Qu and Li proposed the fluorescence detection of PAHs combining CdTe quantum dots (QDs) and cyclodextrins: by varying the cavity size of the cyclodextrin, only a specific PAH could bind, thereby quenching the QDs fluorescence. However, despite the relatively low limit of detection of 0.58 μM for phenanthrene, the method requires a long functionalization procedure.[14]

Low-dimensional materials are ideal scaffolds for the development of highly sensitive and selective sensors which are unexpensive and easy to fabricate, enabling fast and reliable detection of specific chemical species in liquid and gas media.[3,15] Due to their nanometric size and highest surface-to-volume ratio, they exhibit quantum confinement effects

combined with other exclusive properties such as extraordinary thermal and electrical conductivity, markedly high catalytic activity, and unique optical properties making them extremely reactive and suitable candidates for environmental pollution sensing and remediation.[16] In particular, 2D transition metal dichalcogenides (TMDCs) and graphene are considered ideal sensory materials,[17,18] since their unique physical and chemical properties are highly sensitive to environmental changes. Graphene oxide and reduced graphene oxide have been widely exploited for chemical sensing,[19-22] yet the presence of oxygen-containing functional groups on the material's basal plane and edges brings into play background dipole-dipole interactions with multiple potential analytes, thus drastically limiting the selectivity in the sensing process.[23-26]

The successful integration of TMDCs as active materials in functional devices has led to the emergence of specific applications in a multitude of fields including flexible optoelectronics,[27,28] medical diagnosis,[29,30] and chemical sensing.[31-36] Among 2D TMDCs, molybdenum disulfide (MoS_2) has stood out in view of its air stability, which renders it particularly suitable for sensing applications. Moreover, MoS_2 exhibits high density of defects (strain, sulfur vacancies, structural and nano-size defects, *etc*.)[37-43] which are highly reactive sites for unspecific (non-)covalent functionalization with different chemical species.[44,45] For example, the intrinsic defectiveness of MoS_2 was exploited for mercury (II) sensing when integrated in field-effect transistors (FETs).[46] While a great attention has been paid to heavy metals and organic dyes as analytes for chemical sensing, much less effort has been devoted to PAHs whose impact on human health is equally relevant.

Hitherto, PAH sensing was achieved by using cumbersome device architectures.[47-49] Muñoz *et al*. presented an electrochemical impedance spectroscopy sensor, with a complicated heterostructure architecture, operating only in narrow range of concentrations. Baharak Sehatnia *et al.* used square wave voltammetry as detection method, again, using a complicated device structure, obtaining a small range of detection. To the best of our knowledge, the only FET-based device employed to detect PAHs was proposed by Mirzaii Bagolghani and Mohammadi Manesh. In this case, the limit of detection was unfortunately rather high (mM range), even upon using highly complicated device architectures.

Here, we have developed a simple MoS_2 FET sensing platform enabling the identification and quantification of PAHs in water and air. To the best of our knowledge, TMDCS (in particular, MoS_2) integrated in a FET geometry have not been studied in order to electrically sense different PAHs. Our sensing platform, fabricated by means of simple optical lithography protocols, is highly sensitive to naphthalene. X-ray photoelectron spectroscopy (XPS) analysis, along with photoluminescence (PL) measurements and transfer characteristics in FETs showed a notable reduction in MoS_2 defectiveness and a p-type doping upon exposure to PAHs solutions, respectively. The electrical performance of our sensing platform was tested by investigating three key figures of merit, *i.e.* dependence of the response on the analyte type, lowest detectable concentration and reversibility. We were able to correlate the ionization energy (E_I) of the studied PAHs with the magnitude of MoS_2 doping, revealing the strongest signal for naphthalene, whose E_I is the highest among the chosen analytes. In addition, our sensors can detect naphthalene concentrations down to 0.128 ppb, which is below the limits imposed by EPA. Furthermore, they display high reversibility after several exposure/washing cycles.

The fabricated MoS_2 FET-based sensors can also detect PAHs in the gas phase, as demonstrated in a proof-of-concept experiment through *in-situ* naphthalene sublimation. The reversibility of our sensing platform was further supported by performing subsequent sublimation/washing steps. Electrical and Raman spectroscopy readouts confirmed the possibility of using our MoS_2-based sensor as a dual highly sensitive identification platform for naphthalene in air. Such dual sensing, through the collection of independent signals, offers a powerful mean to achieve high selectivity in the sensing process.

RESULTS AND DISCUSSION

The studied sensors consist of MoS_2 flakes integrated into back-gated FET geometries. Figure S1 in the Supporting Information displays a typical sensing device architecture. In particular, it exhibits a scanning electron microscopy (SEM) image of the MoS_2-based FET prior to PAH exposure, along with the optical image of the same few-layer flake. Raman (E^1_{2g}-A_{1g}) peak difference can be correlated with the number of layers of the MoS_2 flake.[50] In our samples, the peak distance is always ranging between 20 and 24 cm^{-1}, corresponding to 1 to 4 layer-thick flakes. Prior to the electrical testing of the device, multiscale characterization (XPS and PL) has been carried out on the same CVD grown MoS_2 films.

X-Ray Photoelectron Spectroscopy Characterization. The defective nature of MoS_2 in its pristine form and when exposed to different PAHs has been studied by high-resolution (HR) XPS by focusing on the S 2p spectrum. In the pristine MoS_2 (Figure 1a) one can deconvolute two main components, *i.e.* the S $2p_{3/2}$ and S $2p_{1/2}$, along with a lower intensity shoulder at ~ 162 eV, the latter being usually associated with defects in the semiconductor lattice, such as structural defects or sulfur vacancies.[51] Generally, the Mo 3d core levels spectrum is also influenced by the presence of defects in the MoS_2 lattice,[52,53] as evidenced in Figure S2a, where the Mo^{4+} $3d_{5/2}$d and Mo^{4+} $3d_{3/2}$d are associated to Mo next to a sulfur vacancy. The intensity of the defective component in the S 2p and Mo 3d XPS spectra (Figures 1b-d, and S2 b-d, respectively) has been recorded after having drop-cast 1 mM acetonitrile solutions of pyrene, phenanthrene, and naphthalene. We found that the adsorption of PAHs induces a significant defect healing, as evidenced by the reduction of the peak contributions of the S 2p defect component and the Mo^{4+} $3d_{5/2}$d and Mo^{4+} $3d_{3/2}$d. The healing appeared to be more effective in the order pyrene < phenanthrene < naphthalene, as shown in Table S1. The functionalization of 2D TMDCs with different molecules has been extensively studied.[54-56] For example, metallophthalocyanines (MPcs) are planar aromatic molecules coordinating a central atom in the inner ring, which are able to reduce the structural defects in TMDCs. In a similar fashion, in this work, the used planar PAHs appeared to be able to induce defect healing in the MoS_2 lattice.

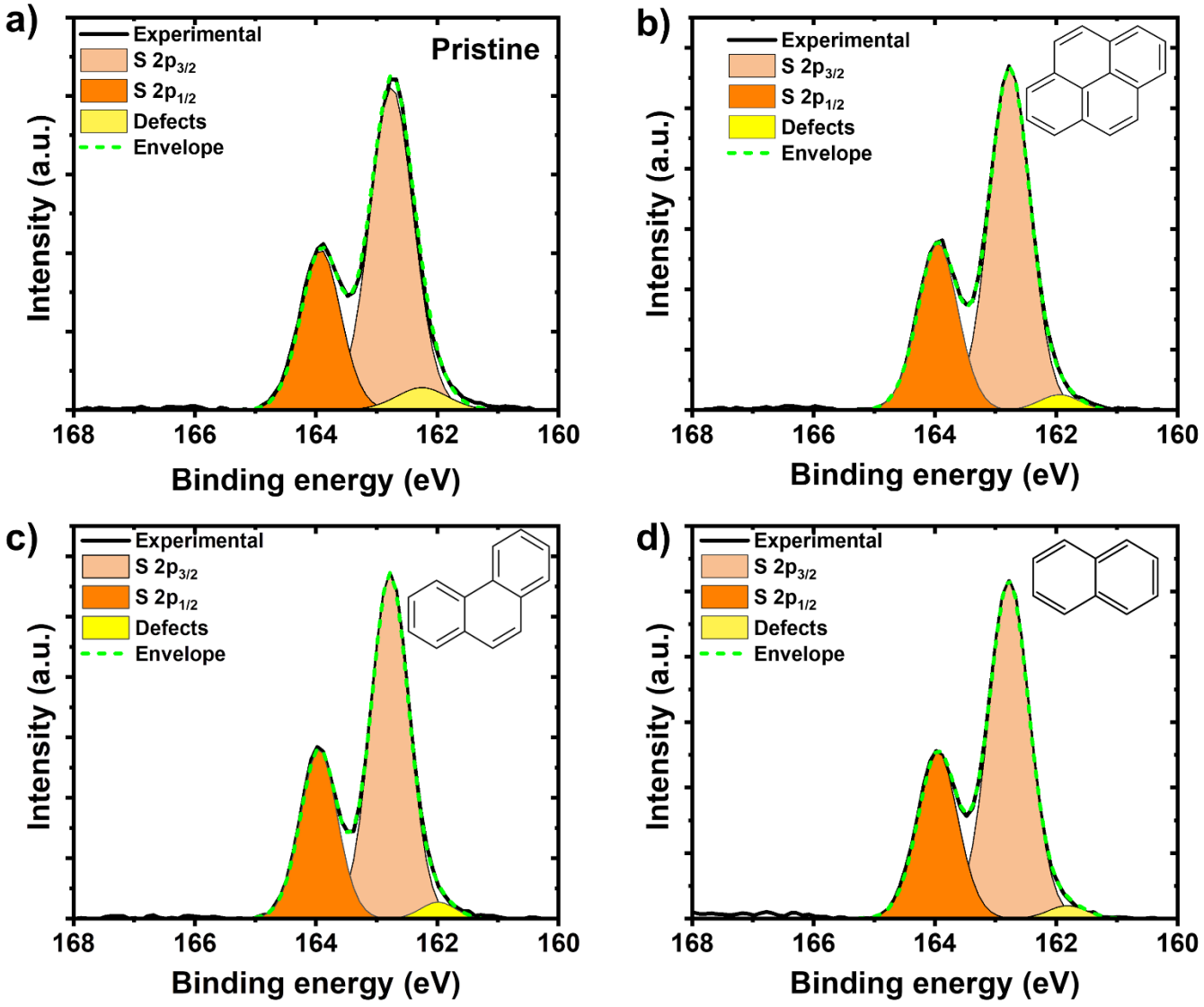

Figure 1. HR-XPS characterization of CVD MoS_2. S 2p signal of **a)** pristine MoS_2, and MoS_2 exposed to 1 mM acetonitrile solution of **b)** pyrene, **c)** phenanthrene, and **d)** naphthalene.

Furthermore, it has been widely reported that thiolated molecules can specifically heal sulfur vacancies in MoS_2.[53, 57, 58] Hence, for the sake of comparison, we have extended our studies to the exposure of MoS_2 to 1-naphthalenethiol. The thiol group effect is clearly demonstrated in Figure S3, with the strong reduction of the defect components' intensity in the Mo 3d and S 2p spectra. The defect healing induced by 1-naphthalenethiol is compared with the other unsubstituted PAHs in Table S1, revealing its higher magnitude, as expected because of the presence of the thiol functional group.

Photoluminescence Characterization. As a semiconductor material, MoS_2 exhibits a strong PL, with a contribution from the so-called A and B excitons, coming from the splitting of the valence band due to the spin-orbit coupling.[59] When MoS_2 is exfoliated in ultrathin layers, this PL becomes more prominent, as a consequence of the shift from indirect to direct bandgap transition moving from multilayer to monolayer.[60] In Figure 2a, a typical PL MoS_2 spectrum is presented, showing the A and B excitonic transitions. In particular, the A exciton can be deconvoluted in two components, the X^- and X^0, namely the negative trion and the neutral exciton, respectively.[61] Pristine MoS_2 has been observed to be intrinsically n-doped, with a PL spectrum dominated by the X^- exciton band (Figure 2a). However, it has been reported that there is a correlation between semiconductor doping and the X^-/X^0 intensity ratio.[62] Mouri *et al.* demonstrated the tunable PL properties of MoS_2 through chemical doping. The PL intensity of MoS_2 was drastically enhanced or suppressed by the adsorption of p- or n-type dopants.

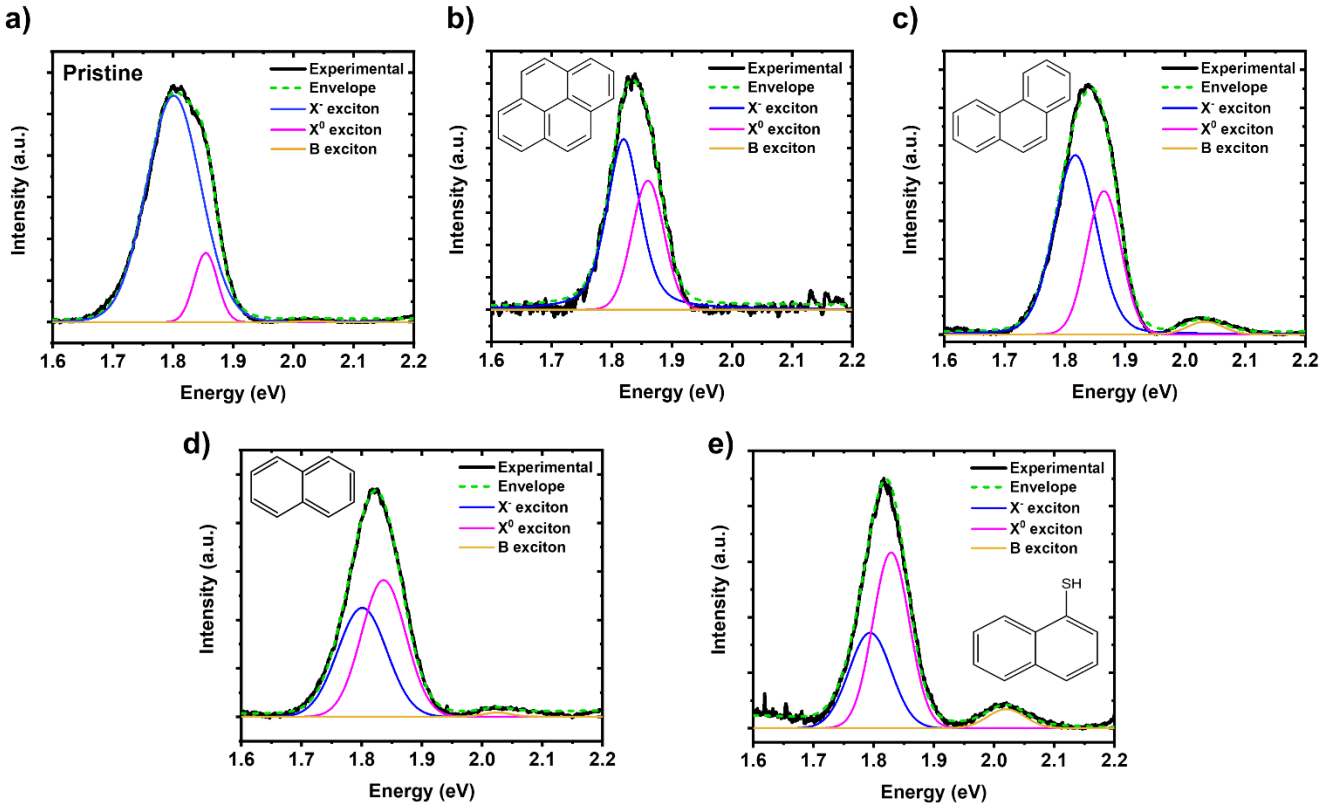

Figure 2. Photoluminescence characterization of **a)** pristine MoS_2 and MoS_2 exposed to 1 mM acetonitrile solution of **b)** pyrene, **c)** phenanthrene, **d)** naphthalene, and **e)** 1 mM ethanol solution of 1-naphthalenethiol. In every case, the A exciton was deconvoluted into two different components: X^- and X^0. X^-/X^0 ratio exhibits a shift towards p-type doping after exposure to different PAHs.

In this work, we observed that the exposure of MoS_2 to the PAHs gives rise to a p-doping, as demonstrated by the gradual increase in the neutral exciton intensity when drop-casting the 1 mM solutions of pyrene, phenanthrene, naphthalene, and 1-naphthalenethiol (Figure 2 b-e, respectively). The X^-/X^0 ratio was calculated for all the samples and we found that a complete inversion takes place in the case of naphthalene and 1-naphthalenethiol exposure (Table S2). Furthermore, the A exciton energy shift has been correlated to the semiconductor doping.[43,62] A blue-shift of 30 meV on average for the A exciton peak has been observed by exposing the MoS_2 to the PAHs, confirming the p-type doping.

The difference observed in the B exciton transitions shown in Figure 2 can be ascribed to the variability in the CVD growth process, leading to small differences in the local optical properties. For this reason, any further assumption has been done on the basis of this exciton band.

Electrical performance of the MoS_2 sensor. To study the performance of the proposed MoS_2-based sensors, we have monitored variations in the threshold voltage (V_{th}), hence using doping changes as gauge. This parameter can be extracted from the FET's transfer characteristic curve, using the extrapolation in the linear region method.[63] We linearly fitted the OFF and ON states of the transistor and determined the interpolation between both fittings.

The performance of our MoS_2-based sensors has been investigated by focusing our attention on three relevant figures of merit: the dependence of the response on the analyte type, the lowest detected concentration, and the reversibility. The study on the dependence of the response on the analyte type is shown in Figure 3. A quantitative insight into the response to different PAH molecules is obtained by following ΔV_{th} upon exposure of the MoS_2 FETs to the four different target analytes at an equal concentration: pyrene, phenanthrene, naphthalene, and 1-naphthalenethiol. The inset shown in Figure 3 represents an example of the FET transfer characteristics before (black) and after (red) PAH exposure. In this case, it corresponds with 1-naphthalenethiol exposure. All the transfer characteristics corresponding to the different analytes can be found in Figures S4-S7. By extrapolating the values of V_{th} one can obtain the ΔV_{th} resulting from the exposure to the analyte, thereby monitoring the doping effect. Figure 3 clearly demonstrates that naphthalene and 1-naphthalenethiol caused stronger doping when compared to other PAHs, such as pyrene or phenanthrene. The stronger interaction between MoS_2 and naphthalene and the consequent greater response shown in Figure 3 (and also in the PL experiments) can be correlated to the higher ionization energy (E_I) of this targeted compound compared to the others (~8.2, ~7.9, ~7.4 eV for naphthalene, phenanthrene and pyrene, respectively).[64,65] It has been indeed experimentally and theoretically found that naphthalene's E_I is higher, implying a lower electron-donating ability of this molecule compared to the other PAHs. In fact, even sharing the same planar geometry, phenanthrene and pyrene are characterized by a more extended π delocalized system, which renders them stronger electron donors. The ionization energy of monolayer MoS_2 has been reported as ~5.7 eV.[66] The higher E_I of naphthalene compared to the other PAHs can explain the higher p-type doping observed in the electrical characterization, as

well as in the PL experiments. These results can be again correlated to the defect healing induced by the PAHs molecule adsorbed on our semiconductor. Amsterdam *et al.* recently demonstrated by gate voltage-dependent measurements and DFT calculations that organic macromolecules as MPcs can stabilize the negatively charged defects in the MoS_2 lattice.[55] Indeed, they found that the positive electrostatic potential of the outer carbon ring of the MPc sitting above the MoS_2 defects stabilizes its negative charge. CoPc (7.46 eV) having higher E_I compared to H_2Pc (7.36 eV)[67] was found as the best stabilizer. Similarly, the trend in ionization energy reported for our PAHs is in good accordance with the trend we observed in the study of the dependence of the response on the analyte type: pyrene< phenanthrene< naphthalene. However, it is not surprising that a markedly higher effect is observed in the case of 1-naphthalenethiol compared to naphthalene as a consequence of the well-known strong interaction of the thiol groups and point defects in TMDCs.[68,69] In this case, the defects present in MoS_2, mainly sulfur vacancies, are acting as anchoring points for the molecular thiol group.

Overall, Figure 3 reveals that, by tracking the change in V_{th}, the different analytes caused a p-type doping of different magnitude. Along the same line, by extrapolating the electron field-effect mobility (μ_{e-}) from the transfer characteristics shown in Figures S4-S7, we could confirm this p-type doping. In all the cases, μ_e was reduced by almost one order of magnitude. The μ_{e-} decreased from 4.2 to 0.5 $cm^2\ V^{-1}\ s^{-1}$ for pyrene, from 7.4 to 2.1 $cm^2\ V^{-1}\ s^{-1}$ for phenanthrene, from 13.2 to 6.8 $cm^2\ V^{-1}\ s^{-1}$ in the case of naphthalene, and from 15.0 to 5.2 $cm^2\ V^{-1}\ s^{-1}$ for 1-naphthalenethiol. Further information about μ_{e-} calculations can be found in the Supplementary Information.

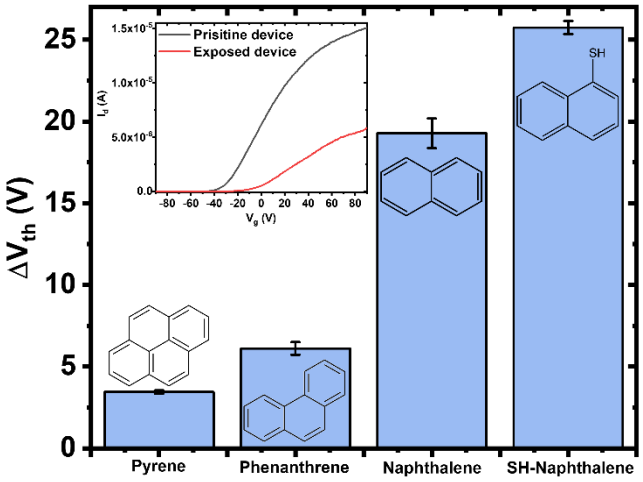

Figure 3. Selectivity study under exposure to different PAHs. Monitored change in threshold voltage (ΔV_{th} in volts) is presented as a function of the selected PAH. Inset represents an example of the MoS_2 FET transfer characteristic curves before and after 1-naphthalenethiol exposure in black and red, respectively.

While being instrumental to understand the role of the defects in the sensing process, it is fair to point out that the detection of 1-naphthalenethiol is not interesting in environmental science, since this compound does not represent a typical contaminant in water. On the other hand, the development of highly performing sensors for naphthalene is particularly interesting because of its impact on health. We have therefore extended our investigation to shed light onto the device sensitivity and reversibility, as presented in Figures 4a and 4b, respectively. Figure 4a displays the calibration curve, obtained by plotting ΔV_{th} as a function of the of the naphthalene content in water, in a wide range of concentrations spanning from 1 μM to 1 nM.

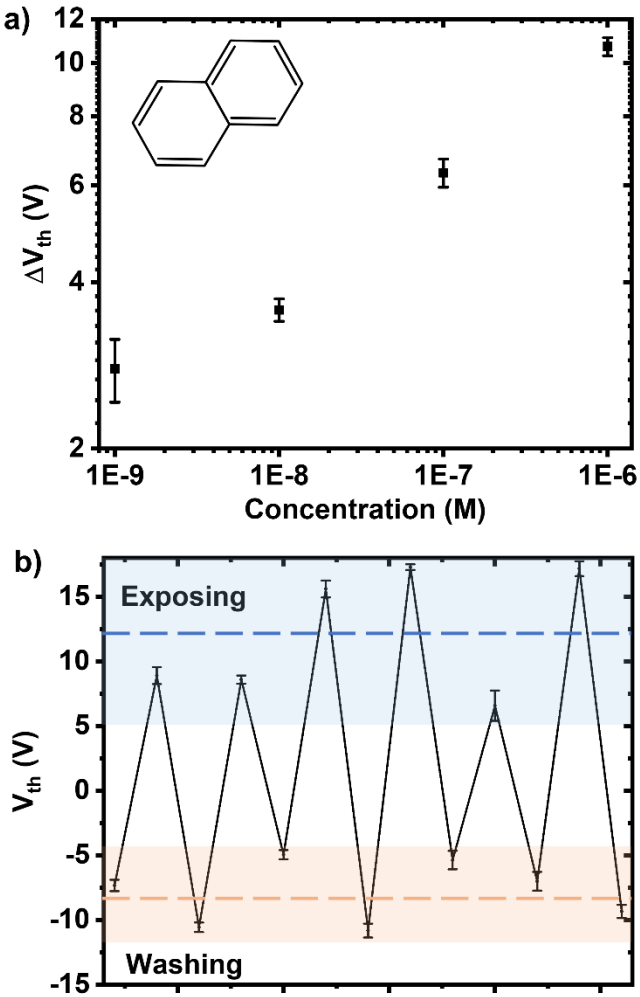

Figure 4. a) Calibration curve for naphthalene. ΔV_{th} as a function of different concentrations, from 1 μM to 1 nM in water, with the device being able to detect concentrations in the nM regime. **b)** Reversibility studies by successive exposure and washing of the MoS_2 FET. Two well-defined levels were observed, highlighted by two background colors. Dashed lines represent the average values of each level. The consecutive exposing/washing cycles showed that the device can be recycled and it is able to restore its initial state.

The log-log plot exhibits a linear trend. With this calibration curve, we can define the lowest concentration that can be detected by our MoS_2-based sensors, being 1 nM. This concentration corresponds to 0.128 ppb, being below the maximum contamination limit of 0.2 ppb imposed by the EPA for drinking water. When compared to the state-of-the-art, our sensing device (i) allows PAH detection in a wider range of concentrations, and (ii) enables to detect lower concentration values. A comparative table can be found in Table S4. Output characteristics before and after naphthalene expo-

sure at 1 μM concentration can be also found in the Supporting Information, Figure S8. Blank experiments corresponding to the exposure of the MoS_2 FETs to water, ethanol and acetonitrile are reported in Figure S9.

Alongside, reversibility is also a critical characteristic of chemical sensors. Figure 4b displays the evolution of V_{th} after successive washing/naphthalene cycles. It reveals a V_{th} shift towards positive values, confirming the previously observed p-type doping, and in good accordance with the PL results. After several cycles, two well-defined levels of doping can be identified, as highlighted by two different colors. The two dashed lines indicate the average V_{th} value for each level (−7.9 V for the washed device and 12.4 V for the exposed device). The reversibility study also proved that the device can restore the initial state after every naphthalene exposure cycle.

Overall, our MoS_2-based sensor has been proved to be highly reversible and capable to detect low concentrations of the chosen analyte with a response driven by the different E_I. On the other hand, we believe that one of the drawbacks of the presented architecture is the lack of identification when performing only electrical sensing. For this reason, we propose the following proof-of-concept experiment.

Proof-of-concept air sensing. Different governmental agencies have established standards for PAHs level in the environment/workplace. For that reason, some organizations such as the OSHA, require strict controls related to the presence of PAHs in the air. In view of the high performance of our MoS_2-based sensors in solution, and the lack of identification of naphthalene, we extended our investigations to proof-of-concept air sensing demonstrations by using the same MoS_2 FETs as a dual detection/identification sensing platform.

Figure S10 shows the scheme of the experimental setup. A homemade closed chamber was built in order to expose our MoS_2-based sensors to naphthalene whose sublimation occurs at 80 °C.[70] Sublimation was achieved by heating the naphthalene crystals at 120 °C. Subsequent sublimation and washing steps were executed. Further experimental details are found in the Experimental Information section.

Interestingly, our MoS_2 FETs were found to operate as dual platform for naphthalene identification in air. The electrical and optical response of the MoS_2 to the exposure to naphthalene gases is portrayed in Figure 5. Figure 5a shows the results of the V_{th} shift in the MoS_2-FET sensor after every sublimation/washing cycle. As expected, the sensor was found to be reversible, undergoing p-type doping which can be recovered to its initial state upon successive steps of naphthalene sublimation and washing, respectively.

Raman spectroscopy is a powerful technique for the analysis of 2D semiconductors, and it is highly relevant for sensing applications.[71] For this reason, we further investigated the performance of our sensor by using the MoS_2 FETs as a Raman identification platform. Figure 5b depicts the μ-Raman spectra of pristine MoS_2 (black), after its exposure to vapors of naphthalene (red) and successive to its washing with acetone and isopropanol (blue). Si Raman peak, originating from the substrate, is evident in all of them at 521 cm^{-1}. The well-studied E^1_{2g} and A_{1g} Raman peaks of MoS_2 are present in the three different spectra and their intensity, as well as the Si one, is highly reduced when naphthalene is sublimating on the sensor surface. Significantly, we observed the presence of new Raman peaks after naphthalene sublimation. These peaks can be identified at 509.7 cm^{-1}, 764.2 cm^{-1},783.8 cm^{-1}, and 1022.2 cm^{-1} and they correspond to the Raman signals coming from the chosen analyte, such as the out-of-plane and in-plane bending vibrations.[72] Upon washing the device, the initial spectrum is completely recovered with the disappearance of all naphthalene peaks. Detailed Raman spectra of the different steps covering wider Raman shift ranges can be found in Figure S11, in the Supporting Information.

Conventional FET-based sensors are typically unable to identify the analyte. However, with the presented proof-of-concept air sensing, the possibility to operate the same device architecture through independent electrical and optical readouts represents a key advantage in order to attain identification in the sensing process.

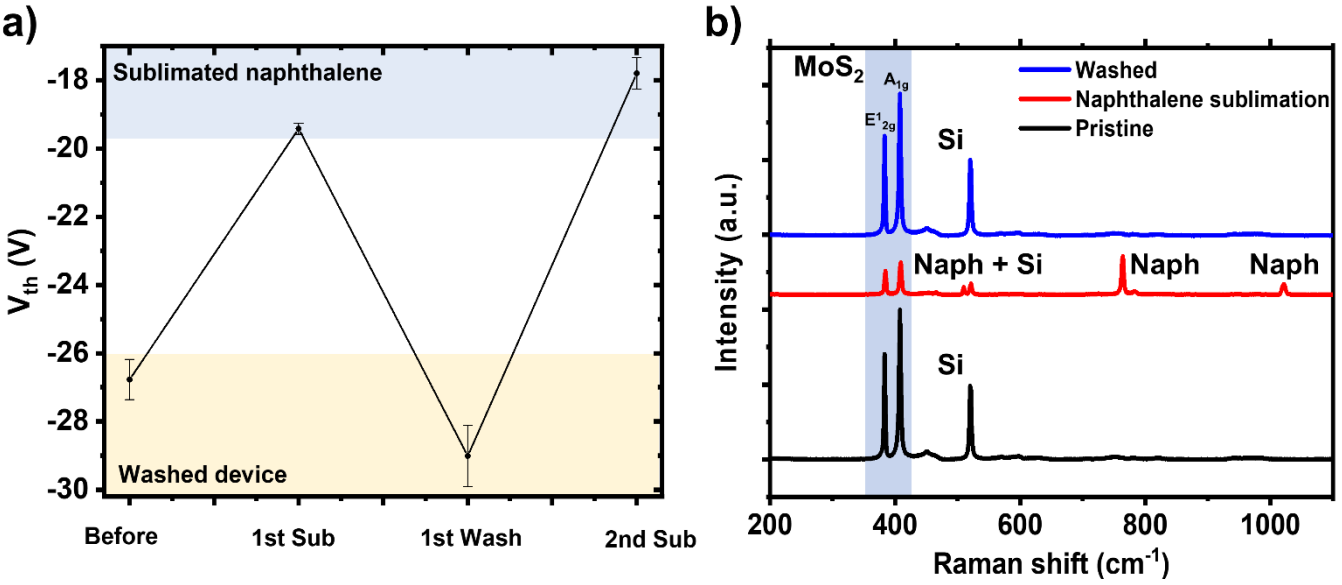

Figure 5. Proof-of-concept PAH air sensing. **a)** Reversibility study after sublimation/washing cycles, obtained monitoring the V_{th} change. **b)**. Raman characterization after every step. Black, red, and blue spectra correspond with the pristine, naphthalene sublimated, and washed device, respectively.

CONCLUSIONS

In this work, we have reported the fabrication of MoS_2-based sensors for the detection of different PAHs with both an electrical and an optical readout. We have focused on four different analytes, *i.e.* pyrene, phenanthrene, naphthalene, and 1-naphthalenethiol.

XPS characterization showed that the intrinsic defectiveness present in MoS_2 decreased upon exposure to the PAHs. The efficiency of the healing process was found to be stronger for naphthalene and 1-naphthalenethiol. PL characterization offered further insight into the interaction mechanism by providing evidence for a dramatic change in the doping of the pristine material after its exposure to different analytes. More specifically, exposure to the PAH determines a p-type doping effect as revealed by both the X^-/X^0 ratio evolution and by a blueshift of 30 meV in the A exciton peak.

Electrical characterization of FET MoS_2 sensors devices revealed a p-type doping after exposure to all the PAHs. Upon monitoring the change in the V_{th}, we observed a greater response to naphthalene and 1-naphthalenethiol due to thiol effect in the latter case. The higher ionization energy of naphthalene compared to pyrene and phenanthrene, along with its less extended π delocalization, make it a better p-dopant. The correlation between ΔV_{th} and E_I values is excellent. It has been proved that the studied naphthalene sensor presented high performance, as it allows the detection of the analyte with a high precision in a broader range of concentrations spanning from 10^{-6} to 10^{-9} M, with the lowest detected value as low as 1 nM in water. Such concentration corresponds to 0.128 ppb, which is below the current health regulations reported by the EPA for drinking water. The reversibility of our sensor was demonstrated by performing consecutive exposure/washing cycles. After every naphthalene exposure, the device was washed, and it showed a full reversibility.

Finally, our sensing platform could successfully detect PAH contaminants in air both with an electrical and an optical readout. The exposure of the transistor to the sublimed analyte was accompanied by a p-doping effect which would be reversed upon washing of the device. Such a reversible sensing could be also detected by μ-Raman spectroscopy by monitoring the appearance and disappearance of naphthalene peaks upon exposure and washing cycles, respectively. Interestingly, the latter study demonstrates that our device can be also used as a Raman identification platform for naphthalene.

The use of defect engineering and controlled healing of MoS_2 upon its interfacing at the (non-)covalent level with ad hoc molecules is a powerful protocol for the development of MoS_2-based sensing platforms combining high selectivity, reversibility, and sensitivity both for detection in water and in air, to meet technological and environmental demands.

EXPERIMENTAL INFORMATION

Materials. Naphthalene, 1-naphthalenethiol, pyrene, and phenanthrene were purchased in Sigma Aldrich. MoS_2 CVD continuous films on Si/SiO_2 substrates were acquired from 6Carbon Technology (Shenzhen). MoS_2 natural crystals were purchased from 2SPI. Few-layer MoS_2 flakes were exfoliated onto substrates purchased from Fraunhofer-Gesellschaft, consisting of a degenerated n-doped silicon substrate capped with 230 nm SiO_2 film and pre-patterned electrodes.

Device PAH exposure. Solutions of naphthalene, pyrene, and phenanthrene were prepared in acetonitrile. Conversely, 1-naphthalenethiol solution was prepared in ethanol.

Response to different analytes and reversibility studies were done by drop-casting 2 μL of different solutions at a fixed concentration of 1 mM. A reversibility study was conducted by washing the exposed devices for 5 minutes in acetone, followed by gently rinsing in isopropanol to remove the acetone residues. Calibration curve was obtained by diluting 1 mM naphthalene solution with water and exposing the devices by drop-casting a 2 μL of the aqueous solutions at different concentrations.

Sublimation experiments were performed at room pressure by heating 75 mg naphthalene crystal at 120 °C for 1 h. After every sublimation experiment, a washing step in acetone was followed by gently rinsing the sensor with isopropanol. The homemade chamber had a diameter of 5 cm and a height of 3 cm.

Device Fabrication. Back-gated FETs were fabricated by using laser optical lithography, followed by thermal evaporation of gold (60 nm). After evaporation, a lift-off was performed in acetone at 50 °C for 1.5 h. After this, annealing at a high vacuum (10^{-6}-10^{-7} mbar) at 180 °C was performed overnight.

Characterization. HR-XPS characterization was carried out on CVD MoS_2 using a Thermo Scientific K-alpha X-ray photoelectron spectrometer, equipped with an aluminum X-ray source (energy 1.4866 keV) at a vacuum level of 10^{-8} -10^{-9} mbar in the analysis chamber. The spot size of the X-ray beam was fixed at 200 μm.

μ-PL and μ-Raman characterizations were performed onto CVD MoS_2 using a Renishaw InVia Reflex system equipped with a confocal microscope and a 2D-CCD camera. Measurements were performed using an excitation wavelength of 532 nm with a 100× objective, and 0.18 mW maximum power. A 300 and 2400 lines per mm grating was used for PL and Raman measurements, respectively.

Electrical transport characterization was conducted in a back-gated geometry using a Keithley 2636B Source Measure Unit, always at room temperature and ambient pressure.

Optical images of MoS_2 FETs were obtained using an optical microscope acquired from Zeiss (Zeiss Axioscope 5). SEM images were acquired using a FEI Quanta 250 FEG Scanning Electron Microscope, operating in a high vacuum mode.

ASSOCIATED CONTENT

Supporting Information: SEM and optical images of MoS_2 FET, Mo 3d XPS HR-spectra after exposure to different PAHs, Mo 3d and S 2p XPS HR-spectra of 1-naphthalenethiol, Tables indicating XPS and PL peak contribution, transfer characteristics related to the selectivity study, mobility calculation, representative output characteristic, blank experiments, state-of-the-art comparison table, air sensing experimental setup, Raman spectra.

This material is available free of charge *via* the Internet at http://pubs.acs.org.

AUTHOR INFORMATION

Corresponding Author

*E-mail: samori@unistra.fr

Author Contributions

F.J.U. and S.G. designed the project. F.J.U. and S.G. carried out all the experiments, analyzed and interpreted the data, and drafted the paper. P.S. coordinated the experimental work and adapted the paper.

The manuscript was written through the contributions of all authors. All authors have approved the final version of the manuscript.

‡ These authors contributed equally.

ACKNOWLEDGMENTS

We acknowledge funding from the European Commission through the ERC project SUPRA2DMAT (GA-833707), the Graphene Flagship Core 3 project (GA-881603) and the Marie Sklodowska-Curie project ULTIMATE (GA-813036) as well as the Agence Nationale de la Recherche through the Interdisciplinary Thematic Institute SysChem via the IdEx Unistra (ANR-10-IDEX-0002) within the program Investissement d'Avenir, the International Center for Frontier Research in Chemistry (icFRC) and the Institut Universitaire de France (IUF).

ABBREVIATIONS

CVD, chemical vapor deposition; E_I, ionization potential; μ_{e^-}, electron mobility; EPA, Environmental Protection Agency; FET, field-effect transistor; HR, high-resolution; MPcs, metallophthalocyanines; QD, quantum dots; OSHA, Occupational Safety and Health Administration; PL, photoluminescence; SEM, scanning electron microscopy; TMDC, transition metal dichalcogenide; V_{th}, threshold voltage; XPS, X-Ray Photoelectron Spectroscopy.

REFERENCES

(1) Lian, L.; Huang, T.; Ke, X.; Ling, Z.; Jiang, W.; Wang, Z.; Song, S.; Li, J.; Zhao, Y.; Gao, H.; et al. Globalization-Driven Industry Relocation Significantly Reduces Arctic PAH Contamination. *Environmental Science & Technology* **2022**, *56* (1), 145-154.

(2) Das, R.; Vecitis, C. D.; Schulze, A.; Cao, B.; Ismail, A. F.; Lu, X.; Chen, J.; Ramakrishna, S. Recent Advances in Nanomaterials for Water Protection and Monitoring. *Chemical Society Reviews* **2017**, *46* (22), 6946-7020, 10.1039/C6CS00921B.

(3) Nagar, A.; Pradeep, T. Clean Water through Nanotechnology: Needs, Gaps, and Fulfillment. *ACS Nano* **2020**, *14* (6), 6420-6435. DOI: 10.1021/acsnano.9b01730.

(4) Bolisetty, S.; Peydayesh, M.; Mezzenga, R. Sustainable Technologies for Water Purification from Heavy Metals: Review and Analysis. *Chemical Society Reviews* **2019**, *48* (2), 463-487.

(5) Draper, W. M.; Li, N.; Solomon, G. M.; Heaney, Y. C.; Crenshaw, R. B.; Hinrichs, R. L.; Chandrasena, R. E. P. Organic Chemical Contaminants in Water System Infrastructure Following Wildfire. *ACS ES&T Water* **2022**, *2* (2), 357-366.

(6) Rota, M.; Bosetti, C.; Boccia, S.; Boffetta, P.; La Vecchia, C. Occupational Exposures to Polycyclic Aromatic Hydrocarbons and Respiratory and Urinary Tract Cancers: an Updated Systematic Review and a Meta-Analysis to 2014. *Archives of Toxicology* **2014**, *88* (8), 1479-1490.

(7) White, A. J.; Gregoire, A. M.; Niehoff, N. M.; Bertrand, K. A.; Palmer, J. R.; Coogan, P. F.; Bethea, T. N. Air Pollution and Breast Cancer Risk in the Black Women's Health Study. *Environmental Research* **2021**, *194*, 110651.

(8) White, A. J.; Bradshaw, P. T.; Herring, A. H.; Teitelbaum, S. L.; Beyea, J.; Stellman, S. D.; Steck, S. E.; Mordukhovich, I.; Eng, S. M.; Engel, L. S.; et al. Exposure to Multiple Sources of Polycyclic Aromatic Hydrocarbons and Breast Cancer Incidence. *Environment International* **2016**, *89-90*, 185-192.

(9) Lübeck, J. S.; Malmquist, L. M. V.; Christensen, J. H. Supercritical Fluid Chromatography for the Analysis of Oxygenated Polycyclic Aromatic Compounds in Unconventional Oils. *Journal of Chromatography A* **2019**, *1589*, 162-172.

(10) Lundstedt, S.; Haglund, P.; Öberg, L. Simultaneous Extraction and Fractionation of Polycyclic Aromatic Hydrocarbons and Their Oxygenated Derivatives in Soil Using Selective Pressurized Liquid Extraction. *Analytical Chemistry* **2006**, *78* (9), 2993-3000.

(11) Li, H.; Wang, L. Highly Selective Detection of Polycyclic Aromatic Hydrocarbons Using Multifunctional Magnetic–Luminescent Molecularly Imprinted Polymers. *ACS Applied Materials & Interfaces* **2013**, *5* (21), 10502-10509.

(12) Yu, Z.; Grasso, M. F.; Sorensen, H. H.; Zhang, P. Ratiometric SERS Detection of Polycyclic Aromatic Hydrocarbons Assisted by β-Cyclodextrin-Modified Gold Nanoparticles. *Microchimica Acta* **2019**, *186* (6), 391.

(13) Stanley, S.; Percival, C. J.; Auer, M.; Braithwaite, A.; Newton, M. I.; McHale, G.; Hayes, W. Detection of Polycyclic Aromatic Hydrocarbons Using Quartz Crystal Microbalances. *Analytical Chemistry* **2003**, *75* (7), 1573-1577.

(14) Qu, F.; Li, H. Selective Molecular Recognition of Polycyclic Aromatic Hydrocarbons Using CdTe Quantum Dots with Cyclodextrin As Supramolecular Nano-Sensitizers in Water. *Sensors and Actuators B: Chemical* **2009**, *135* (2), 499-505.

(15) Gullace, S.; Montes-García, V.; Martín, V.; Larios, D.; Girelli Consolaro, V.; Obelleiro, F.; Calogero, G.; Casalini, S.; Samorì, P. Universal Fabrication of Highly Efficient Plasmonic Thin-Films for Label-Free SERS Detection. *Small* **2021**, *17* (33), 2100755.

(16) Baig, N.; Kammakakam, I.; Falath, W. Nanomaterials: a Review of Synthesis Methods, Properties, Recent Progress, and Challenges. *Materials Advances* **2021**, *2* (6), 1821-1871.
(17) Anichini, C.; Czepa, W.; Pakulski, D.; Aliprandi, A.; Ciesielski, A.; Samorì, P. Chemical Sensing with 2D Materials. *Chemical Society Reviews* **2018**, *47* (13), 4860-4908.
(18) Moore, D. C.; Jawaid, A.; Busch, R.; Brothers, M.; Miesle, P.; Miesle, A.; Rao, R.; Lee, J.; Beagle, L. K.; Motala, M.; et al. Ultrasensitive Molecular Sensors Based on Real-Time Impedance Spectroscopy in Solution-Processed 2D Materials. *Advanced Functional Materials* **2022**, *32* (12), 2106830.
(19) Robinson, J. T.; Perkins, F. K.; Snow, E. S.; Wei, Z.; Sheehan, P. E. Reduced Graphene Oxide Molecular Sensors. *Nano Letters* **2008**, *8* (10), 3137-3140.
(20) Kim, Y. H.; Kim, S. J.; Kim, Y.-J.; Shim, Y.-S.; Kim, S. Y.; Hong, B. H.; Jang, H. W. Self-Activated Transparent All-Graphene Gas Sensor with Endurance to Humidity and Mechanical Bending. *ACS Nano* **2015**, *9* (10), 10453-10460.
(21) Choi, H.; Choi, J. S.; Kim, J.-S.; Choe, J.-H.; Chung, K. H.; Shin, J.-W.; Kim, J. T.; Youn, D.-H.; Kim, K.-C.; Lee, J.-I.; et al. Flexible and Transparent Gas Molecule Sensor Integrated with Sensing and Heating Graphene Layers. *Small* **2014**, *10* (18), 3685-3691.
(22) Chen, J.; Pu, H.; Hersam, M. C.; Westerhoff, P. Molecular Engineering of 2D Nanomaterial Field-Effect Transistor Sensors: Fundamentals and Translation Across the Innovation Spectrum. *Advanced Materials* **2022**, *34* (3), 2106975.
(23) Black, A.; Urbanos, F. J.; Osorio, M. R.; Miranda, R.; Vázquez de Parga, A. L.; Granados, D. Encapsulating Chemically Doped Graphene via Atomic Layer Deposition. *ACS Applied Materials & Interfaces* **2018**, *10* (9), 8190-8196.
(24) Kidambi, P. R.; Bayer, B. C.; Blume, R.; Wang, Z.-J.; Baehtz, C.; Weatherup, R. S.; Willinger, M.-G.; Schloegl, R.; Hofmann, S. Observing Graphene Grow: Catalyst–Graphene Interactions During Scalable Graphene Growth on Polycrystalline Copper. *Nano Letters* **2013**, *13* (10), 4769-4778.
(25) Furlan de Oliveira, R.; Montes-García, V.; Ciesielski, A.; Samorì, P. Harnessing Selectivity in Chemical Sensing via Supramolecular Interactions: from Functionalization of Nanomaterials to Device Applications. *Materials Horizons* **2021**, *8* (10), 2685-2708.
(26) Shams, M.; Guiney, L. M.; Huang, L.; Ramesh, M.; Yang, X.; Hersam, M. C.; Chowdhury, I. Influence of Functional Groups on the Degradation of Graphene Oxide Nanomaterials. *Environmental Science: Nano* **2019**, *6* (7), 2203-2214.
(27) Pu, J.; Yomogida, Y.; Liu, K.-K.; Li, L.-J.; Iwasa, Y.; Takenobu, T. Highly Flexible MoS_2 Thin-Film Transistors with Ion Gel Dielectrics. *Nano Letters* **2012**, *12* (8), 4013-4017.
(28) Schneider, D. S.; Grundmann, A.; Bablich, A.; Passi, V.; Kataria, S.; Kalisch, H.; Heuken, M.; Vescan, A.; Neumaier, D.; Lemme, M. C. Highly Responsive Flexible Photodetectors Based on MOVPE Grown Uniform Few-Layer MoS_2. *ACS Photonics* **2020**, *7* (6), 1388-1395.
(29) He, X.-P.; Tian, H. Photoluminescence Architectures for Disease Diagnosis: from Graphene to Thin-Layer Transition Metal Dichalcogenides and Oxides. *Small* **2016**, *12* (2), 144-160.
(30) Zhu, S.; Gong, L.; Xie, J.; Gu, Z.; Zhao, Y. Design, Synthesis, and Surface Modification of Materials Based on Transition-Metal Dichalcogenides for Biomedical Applications. *Small Methods* **2017**, *1* (12), 1700220.
(31) Zhao, J.; Li, N.; Yu, H.; Wei, Z.; Liao, M.; Chen, P.; Wang, S.; Shi, D.; Sun, Q.; Zhang, G. Highly Sensitive MoS_2 Humidity Sensors Array for Noncontact Sensation. *Advanced Materials* **2017**, *29* (34), 1702076.
(32) Zhang, D.; Sun, Y. e.; Li, P.; Zhang, Y. Facile Fabrication of MoS_2-Modified SnO_2 Hybrid Nanocomposite for Ultrasensitive Humidity Sensing. *ACS Applied Materials & Interfaces* **2016**, *8* (22), 14142-14149.
(33) Guo, S.; Yang, D.; Zhang, S.; Dong, Q.; Li, B.; Tran, N.; Li, Z.; Xiong, Y.; Zaghloul, M. E. Development of a Cloud-Based Epidermal $MoSe_2$ Device for Hazardous Gas Sensing. *Advanced Functional Materials* **2019**, *29* (18), 1900138.
(34) Kumar, R.; Zheng, W.; Liu, X.; Zhang, J.; Kumar, M. MoS_2-Based Nanomaterials for Room-Temperature Gas Sensors. *Advanced Materials Technologies* **2020**, 5, 1901062.
(35) Pham, T.; Li, G.; Bekyarova, E.; Itkis, M. E.; Mulchandani, A. MoS_2-Based Optoelectronic Gas Sensor with Sub-Parts-per-Billion Limit of NO_2 Gas Detection. *ACS Nano* **2019**, 13, 3196-3205.
(36) Shokri, A.; Salami, N. Gas Sensor Based on MoS_2 Monolayer. *Sensors and Actuators B: Chemical* **2016**, 236, 378-385.
(37) Rhodes, D.; Chae, S. H.; Ribeiro-Palau, R.; Hone, J. Disorder in Van der Waals Heterostructures of 2D Materials. *Nature Materials* **2019**, *18* (6), 541-549.
(38) Zhou, W.; Zou, X.; Najmaei, S.; Liu, Z.; Shi, Y.; Kong, J.; Lou, J.; Ajayan, P. M.; Yakobson, B. I.; Idrobo, J.-C. Intrinsic Structural Defects in Monolayer Molybdenum Disulfide. *Nano Letters* **2013**, *13* (6), 2615-2622.
(39) Ippolito, S.; Samorì, P. Defect Engineering Strategies Toward Controlled Functionalization of Solution-Processed Transition Metal Dichalcogenides. *Small Science* **2022**, *2* (4), 2100122.
(40) Li, L.; Qin, Z.; Ries, L.; Hong, S.; Michel, T.; Yang, J.; Salameh, C.; Bechelany, M.; Miele, P.; Kaplan, D.; et al. Role of Sulfur Vacancies and Undercoordinated Mo Regions in MoS_2 Nanosheets Toward the Evolution of Hydrogen. *ACS Nano* **2019**, *13* (6), 6824-6834.
(41) Hong, J.; Hu, Z.; Probert, M.; Li, K.; Lv, D.; Yang, X.; Gu, L.; Mao, N.; Feng, Q.; Xie, L.; et al. Exploring Atomic Defects in Molybdenum Disulphide Monolayers. *Nature Communications* **2015**, *6* (1), 6293.
(42) Hu, Z.; Wu, Z.; Han, C.; He, J.; Ni, Z.; Chen, W. Two-Dimensional Transition Metal Dichalcogenides: Interface and Defect Engineering. *Chemical Society Reviews* **2018**, *47* (9), 3100-3128.
(43) Urbanos, F. J.; Black, A.; Bernardo-Gavito, R.; Vázquez de Parga, A. L.; Miranda, R.; Granados, D. Electrical and Geometrical Tuning of MoS_2 Field Effect Transistors via Direct Nanopatterning. *Nanoscale* **2019**, *11* (23), 11152-11158.

(44) Nguyen, E. P.; Carey, B. J.; Ou, J. Z.; van Embden, J.; Gaspera, E. D.; Chrimes, A. F.; Spencer, M. J. S.; Zhuiykov, S.; Kalantar-zadeh, K.; Daeneke, T. Electronic Tuning of 2D MoS_2 Through Surface Functionalization. *Advanced Materials* **2015**, *27* (40), 6225-6229.
(45) Förster, A.; Gemming, S.; Seifert, G.; Tománek, D. Chemical and Electronic Repair Mechanism of Defects in MoS_2 Monolayers. *ACS Nano* **2017**, *11* (10), 9989-9996.
(46) Urbanos, F. J.; Gullace, S.; Samorì, P. Field-Effect-Transistor-Based Ion Sensors: Ultrasensitive Mercury(ii) Detection via Healing MoS_2 Defects. *Nanoscale* **2021**, *13* (46), 19682-19689.
(47) Muñoz, J.; Campos-Lendinez, Á.; Crivillers, N.; Mas-Torrent, M. Selective Discrimination of Toxic Polycyclic Aromatic Hydrocarbons in Water by Targeting π-Stacking Interactions. *ACS Applied Materials & Interfaces* **2020**, *12* (23), 26688-26693.
(48) Sehatnia, B.; Sabzi, R. E.; Kheiri, F.; Nikoo, A. Sensitive Molecular Determination of Polycyclic Aromatic Hydrocarbons Based on Thiolated Calix[4]arene and CdSe Quantum Dots (QDs). *Journal of Applied Electrochemistry* **2014**, *44* (6), 727-733.
(49) Mirzaii Babolghani, F.; Mohammadi-Manesh, E. Simulation and Experimental Study of FET Biosensor to Detect Polycyclic Aromatic Hydrocarbons. *Applied Surface Science* **2019**, *488*, 662-670.
(50) Li, H.; Zhang, Q.; Yap, C. C. R.; Tay, B. K.; Edwin, T. H. T.; Olivier, A.; Baillargeat, D. From Bulk to Monolayer MoS_2: Evolution of Raman Scattering. *Advanced Functional Materials* **2012**, 22, 1385-1390.
(51) Ippolito, S.; Kelly, A. G.; Furlan de Oliveira, R.; Stoeckel, M.-A.; Iglesias, D.; Roy, A.; Downing, C.; Bian, Z.; Lombardi, L.; Samad, Y. A.; et al. Covalently Interconnected Transition Metal Dichalcogenide Networks via Defect Engineering for High-Performance Electronic Devices. *Nature Nanotechnology* **2021**, *16* (5), 592-598.
(52) Kim, I. S.; Sangwan, V. K.; Jariwala, D.; Wood, J. D.; Park, S.; Chen, K.-S.; Shi, F.; Ruiz-Zepeda, F.; Ponce, A.; Jose-Yacaman, M.; et al. Influence of Stoichiometry on the Optical and Electrical Properties of Chemical Vapor Deposition Derived MoS_2. *ACS Nano* **2014**, *8* (10), 10551-10558.
(53) Syari'ati, A.; Kumar, S.; Zahid, A.; Ali El Yumin, A.; Ye, J.; Rudolf, P. Photoemission Spectroscopy Study of Structural Defects in Molybdenum Disulfide (MoS_2) Grown by Chemical Vapor Deposition (CVD). *Chemical Communications* **2019**, *55* (70), 10384-10387.
(54) Ahn, H.; Huang, Y.-C.; Lin, C.-W.; Chiu, Y.-L.; Lin, E.-C.; Lai, Y.-Y.; Lee, Y.-H. Efficient Defect Healing of Transition Metal Dichalcogenides by Metallophthalocyanine. *ACS Applied Materials & Interfaces* **2018**, *10* (34), 29145-29152.
(55) Amsterdam, S. H.; Stanev, T. K.; Wang, L.; Zhou, Q.; Irgen-Gioro, S.; Padgaonkar, S.; Murthy, A. A.; Sangwan, V. K.; Dravid, V. P.; Weiss, E. A.; et al. Mechanistic Investigation of Molybdenum Disulfide Defect Photoluminescence Quenching by Adsorbed Metallophthalocyanines. *Journal of the American Chemical Society* **2021**, *143* (41), 17153-17161.
(56) Zhang, H.; Choi, J.; Ramani, A.; Voiry, D.; Natoli, S. N.; Chhowalla, M.; McMillin, D. R.; Choi, J. H. Engineering Chemically Exfoliated Large-Area Two-Dimensional MoS_2 Nanolayers with Porphyrins for Improved Light Harvesting. *ChemPhysChem* **2016**, *17* (18), 2854-2862.
(57) Feng, S.; Tan, J.; Zhao, S.; Zhang, S.; Khan, U.; Tang, L.; Zou, X.; Lin, J.; Cheng, H.-M.; Liu, B. Synthesis of Ultrahigh-Quality Monolayer Molybdenum Disulfide Through In Situ Defect Healing with Thiol Molecules. *Small* **2020**, *16* (35), 2003357.
(58) Zhao, Y.; Gobbi, M.; Hueso, L. E.; Samorì, P. Molecular Approach to Engineer Two-Dimensional Devices for CMOS and Beyond-CMOS Applications. *Chemical Reviews* **2022**, *122* (1), 50-131.
(59) Ben Amara, I.; Ben Salem, E.; Jaziri, S. Optoelectronic Response and Excitonic Properties of Monolayer MoS_2. *Journal of Applied Physics* **2016**, *120* (5), 051707.
(60) Splendiani, A.; Sun, L.; Zhang, Y.; Li, T.; Kim, J.; Chim, C.-Y.; Galli, G.; Wang, F. Emerging Photoluminescence in Monolayer MoS_2. *Nano Letters* **2010**, *10* (4), 1271-1275.
(61) Mak, K. F.; He, K.; Lee, C.; Lee, G. H.; Hone, J.; Heinz, T. F.; Shan, J. Tightly Bound Trions in Monolayer MoS_2. *Nature Materials* **2013**, *12* (3), 207-211.
(62) Mouri, S.; Miyauchi, Y.; Matsuda, K. Tunable Photoluminescence of Monolayer MoS_2 via Chemical Doping. *Nano Letters* **2013**, *13* (12), 5944-5948.
(63) Ortiz-Conde, A.; García Sánchez, F. J.; Liou, J. J.; Cerdeira, A.; Estrada, M.; Yue, Y. A review of recent MOSFET Threshold Voltage Extraction Methods. *Microelectronics Reliability* **2002**, *42* (4), 583-596.
(64) Bachman, J. C.; Kavian, R.; Graham, D. J.; Kim, D. Y.; Noda, S.; Nocera, D. G.; Shao-Horn, Y.; Lee, S. W. Electrochemical Polymerization of Pyrene Derivatives on Functionalized Carbon Nanotubes for Pseudocapacitive Electrodes. *Nature Communications* **2015**, *6* (1), 7040.
(65) Holm, A. I. S.; Johansson, H. A. B.; Cederquist, H.; Zettergren, H. Dissociation and Multiple Ionization Energies for Five Polycyclic Aromatic Hydrocarbon Molecules. *The Journal of Chemical Physics* **2011**, *134* (4), 044301.
(66) Keyshar, K.; Berg, M.; Zhang, X.; Vajtai, R.; Gupta, G.; Chan, C. K.; Beechem, T. E.; Ajayan, P. M.; Mohite, A. D.; Ohta, T. Experimental Determination of the Ionization Energies of $MoSe_2$, WS_2, and MoS_2 on SiO_2 Using Photoemission Electron Microscopy. *ACS Nano* **2017**, *11* (8), 8223-8230.
(67) Eley, D. D.; Hazeldine, D. J.; Palmer, T. F. Mass Spectra, Ionisation Potentials and Related Properties of Metal-Free and Transition Metal Phthalocyanines. *Journal of the Chemical Society, Faraday Transactions 2: Molecular and Chemical Physics* **1973**, *69* (0), 1808-1814.
(68) Bertolazzi, S.; Bonacchi, S.; Nan, G.; Pershin, A.; Beljonne, D.; Samorì, P. Engineering Chemically Active Defects in Monolayer MoS_2 Transistors via Ion-Beam Irradiation and Their Healing via Vapor Deposition of Alkanethiols. *Advanced Materials* **2017**, *29* (18), 1606760.
(69) Yu, Z.; Pan, Y.; Shen, Y.; Wang, Z.; Ong, Z.-Y.; Xu, T.; Xin, R.; Pan, L.; Wang, B.; Sun, L.; et al. Towards Intrinsic Charge Transport in Monolayer Molybdenum Disulfide by Defect and Interface Engineering. *Nature Communications* **2014**, *5* (1), 5290.
(70) Souza Mendes, P. R. The Naphthalene Sublimation Technique. *Experimental Thermal and Fluid Science* **1991**, *4* (5), 510-523.

(71) Koklioti, M. A.; Bittencourt, C.; Noirfalise, X.; Saucedo-Orozco, I.; Quintana, M.; Tagmatarchis, N. Nitrogen-Doped Silver-Nanoparticle-Decorated Transition-Metal Dichalcogenides as Surface-Enhanced Raman Scattering Substrates for Sensing Polycyclic Aromatic Hydrocarbons. *ACS Applied Nano Materials* **2018**, *1* (7), 3625-3635.
(72) Martin, J. M. L.; El-Yazal, J.; François, J.-P. Structure and Vibrational Spectrum of Some Polycyclic Aromatic Compounds Studied by Density Functional Theory. 1. Naphthalene, Azulene, Phenanthrene, and Anthracene. *The Journal of Physical Chemistry* **1996**, *100* (38), 15358-15367.